Advances in Water Resources 178 (2023) 104441

Contents lists available at ScienceDirect

Advances in Water Resources

journal homepage: www.elsevier.com/locate/advwatres

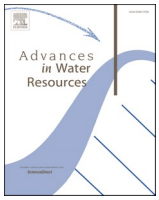

Exploring the Signal Filtering Properties of Idealized Watersheds Using Spectral Analysis

Abram Farley , Laura E. Condon

Department of Hydrology and Atmospheric Sciences, The University of Arizona

A B S T R A C T

Watersheds act as low-pass filters, damping and attenuating climatic signals as water moves through the surface and subsurface. This is a well observed phenomenon; however, the ways in which watershed properties control the nature of this filtering are less well documented, especially with respect to groundwater surface water interactions. Here, we use a physically based groundwater surface water model to simulate idealized hillslope ensembles with varying watershed properties (hillslope slope, hydraulic conductivity, and precipitation magnitude) to quantitively explore the impact of watershed configuration on temporal filtering in both the surface and subsurface. To limit the complexities of this system an idealized titled-v domain is used. Multi-decadal simulations (95 years) are run, and then power spectral densities and transfer functions are used to quantify the temporal dynamics and damping of each simulation. Overall, we show that the degree of filtering and the degree of signal transformation is controlled by the total time spent in the subsurface and the degree of groundwater surface water exchanges. The ratio of precipitation to hydraulic conductivity controls the partitioning between infiltration and runoff. Greater infiltration results in less filtering in the subsurface and more filtering in streamflow. For a given precipitation conductivity ratio, deeper water table depths lead to greater streamflow filtering for periods less than 5 years. For time periods greater than 5 years the streamflow filtering is most strongly related to hydraulic conductivity which controls the baseflow dynamics. The majority of the input signal is filtered in the subsurface for short periods less than one year. For longer time scales, hydraulic conductivity is found to be the primary control of filtering and power shift taking place in the subsurface with larger conductivities correlated to less filtering and less of a signal transformation. Deeper water table depths lead to more signal transformation in saturated storage but are not correlated to filtering in unsaturated storage. This is likely due to counteracting effects of higher conductivity (which decreases filtering) and deeper water table depths (which increase filtering).

1. Introduction

Watersheds can be conceptualized as a series of filters that damp and attenuate climatic signals. Precipitation signals (i.e., watershed inputs) are often considered to be white noise (Delworth & Manabe, 1988; Katul et al., 2007); however, the resulting watershed outflow time series are more organized with greater memory, and decreased noise. Input signals get progressively filtered as they move through the watershed system resulting in decreased high frequency variability moving downstream along a river or working down into the subsurface (Li & Zhang, 2007; Matsoukas et al., 2000; Yang et al., 2018).

While high frequency filtering is a well observed phenomenon (Delworth & Manabe, 1988; Katul et al., 2007; Xiuyu Liang et al., 2016) the watershed characteristics which control the properties of this filtering are less well understood and often difficult to parse out in real world, complex systems (Sauquet et al., 2008). Previous work has utilized both numerical and observational data to demonstrate this filtering (Katul et al., 2007; Li & Zhang, 2007; Matsoukas et al., 2000; Pandey et al., 1998; Yang et al., 2018; Zhang & Yang, 2010); however, considering integrated groundwater behavior with numerical simulations has not yet been quantitatively explored.

As noted above, filtering occurs progressively as signals propagate through watersheds resulting in a spectral shift towards low frequency variability. Streamflow responds almost immediately to precipitation and as a result precipitation generated runoff has a greater variance and is more representative of the climatic input than other hydrologic signals. Still, filtering and signal transformations do occur as this precipitation works its way through the stream network and slow processes like baseflow further smooth the streamflow time series. As a result, streamflow still exhibits filtering of the high frequency variability and longer memory than precipitation (Gall et al., 2013; Guan et al., 2011; Pandey et al., 1998; Sauquet et al., 2008; Tessier et al., 1996).

The subsurface is one of the most significant sources of damping in the system. It has been demonstrated that the white noise precipitation signal gets reddened as the high frequencies are damped even in shallow soil moisture time series (Delworth & Manabe, 1988; Katul et al., 2007; Vinnikov et al., 1996). As we move deeper into soil profile the soil moisture variability and correlation with climatic signal decreases indicating greater buffering as high-frequency fluctuations are damped (Amenu et al., 2005; Entin et al., 2000; Manfreda, 2007; Wu et al.,

E-mail address: ajfarley@gmail.com (A. Farley).

https://doi.org/10.1016/j.advwatres.2023.104441
Received 5 November 2022; Received in revised form 12 March 2023; Accepted 11 April 2023
Available online 26 April 2023

2002). It has been shown that the decay time scales (time for a signal to decrease to 1/e its original signal) of soil moisture as well as the temporal scaling both increase with depth in the subsurface (Wu & Dickinson, 2004; Yang et al., 2018). Moving deeper into the subsurface, the temporal scaling continues to increase with depth (Yang et al., 2018) and subsurface acts as a fractal filter (Li & Zhang, 2007; Yang et al., 2018; Zhang & Schilling, 2005).

While the general trends of increased filtering and reddening of the signal with depth are well established, the impact of watershed characteristics on this behavior is less well understood. Many observational studies of streamflow have found that there is temporal scaling present in the streamflow spectra and that there exists a breakpoint or crossover point where the scaling exponent shifts (Gall et al., 2013; Guan et al., 2011; Pandey et al., 1998; Sauquet et al., 2008; Tessier et al., 1996); however, the value of the scaling exponent of streamflow and the frequency of the break point vary from study to study based on the temporal resolution of the data and the differences in the catchments studied. Some studies have found that basin size does not affect the spectral scaling of stream flow over a large spread of basin sizes (Pandey et al., 1998; Tessier et al., 1996). While another study found the size of the drainage area does affect the scaling parameters (Özger et al., 2013).

Similarly, several studies have explored the controls of temporal scaling in groundwater. Condon and Maxwell (2014) compared scaling responses of latent heat and water table depth to changes in irrigation. They found both that water table depth exhibited more scaling than latent heat and that breaks in scaling for the water table depth depended on proximity to the river. Areas more closely connected to the river had breaks in scaling whereas other areas did not have scaling breaks. Zhang and Li (2005) used a 1D transient model with both homogenous and heterogenous hydraulic conductivities to look at the temporal scaling of groundwater head. They found that switching between the two subsurface configurations has little effect on the scaling factor of groundwater head. In Xiuyu Liang and Zhang (2013), a bounded unconfined aquifer was investigated by developing a theoretical formula for the input and output spectra of their domain. They found that the characteristic time of an aquifer controls the scaling of the hydraulic head which is a function of both the drainage area, hydraulic conductivity, and specific yield. Related studies (X. Liang & Zhang, 2015; Xiuyu Liang et al., 2016) found that while heterogeneity and boundary conditions affect the hydraulic head scaling, the areal recharge has a more significant influence. Furthermore, Zhang and Yang (2010) systematically altered hydraulic conductivity for a watershed simulation using MODFLOW 2000 to explore connections between conductivity and temporal scaling in the subsurface. They found that the influence of hydraulic conductivity on groundwater head scaling varied based on the scenario (constant river stage vs varied river stage and homogeneous vs heterogeneous subsurface). For the homogenous scenario with constant river stage, it was found that as K increased the groundwater head spectra shifted down indicating more filtering occurred across all frequencies.

Still few studies have systematically explored the impact of groundwater and groundwater surface water interactions on temporal scaling and memory across both surface and subsurface systems. Conceptually, we expect groundwater configuration to influence streamflow scaling. We know that water table configuration and groundwater fluxes are dependent on topography, recharge rate, and hydraulic conductivity (Freeze & Witherspoon, 1967; Gleeson & Manning, 2008; Gleeson et al., 2011; Haitjema & Mitchell-Bruker, 2005; Reed M Maxwell et al., 2016; Tóth, 1963). High recharge rates, low hydraulic conductivities, and shallow topography generally cause shallower water tables. Whereas low recharge rates, high hydraulic conductivities and steep topography generally cause deep water table depths. Furthermore, its established that shallow water tables lead to more local flow paths and deeper water tables lead to more regional flow paths (Freeze & Witherspoon, 1967; Gleeson & Manning, 2008; Haitjema & Mitchell-Bruker, 2005; Tóth, 1963), and we would expect to see greater damping for longer flow paths than shorter flow paths (Li & Zhang, 2007; Yang et al., 2018).

Due to the complexity, heterogeneity, and interconnectedness of watersheds, the controlling characteristics of the temporal scaling in a watershed can be difficult to isolate. This study builds upon this previous research, by using a simple idealized tilted-v watershed domain and a fully integrated hydrology model to quantify changes in temporal scaling as a function of both surface and subsurface watershed characteristics. There are many interesting hydraulic components which could be analyzed, in this research we elect to explore the scaling behaviors in streamflow, soil moisture, unsaturated and saturated groundwater storage and compare the dynamics of these system components as well as the varying impacts of watershed characteristics on their signal transformation and filtering properties.

2. Methods

An ensemble of idealized simulations was designed to investigate the relationship between watershed properties, signal filtering and memory. The simulations were run using an idealized tilted-v domain (Section 2.1) and an integrated physical hydrology model ParFlow (Section 2.2). Adjustable parameters of the watershed such as hydraulic conductivity, precipitation, and topographic slopes (Section 2.3) were altered to develop an ensemble of simulations (Section 2.4). Hydrologic responses from the simulations such as streamflow, storages, water table depth were calculated for each of the runs (Section 2.5) and the temporal dynamics of the simulations were then quantitatively evaluated using a range of spectral methods, including power spectral density (Section 2.6) and transfer functions (Section 2.7). Finally, memory metrics were computed to compare the input precipitation time series with the resulting streamflow and storage time series (Section 2.8).

2.1. Baseline Configuration

In order to investigate the hydrologic controls of filtering, we chose this simple watershed design so we could systematically manipulate the characteristics with a small number of parameters, and because the tilted-v domain is a commonly used benchmark problem in hydrology (Carlier et al., 2018; S. Kollet et al., 2017; Reed M. Maxwell et al., 2014; Rahman et al., 2019). The tilted-v (shown in Fig. 1) has two hillslopes of equal length and width (2000m) with a river channel (40m) running between the two hillslopes and is of uniform thickness (100m). The domain was discretized into cells with lengths and widths of 40m (dx = dy = 40m) and thicknesses of 2.5m (dz = 2.5m). The slope of the two hillslopes (HS) varied while the slope along the axis of the river, River

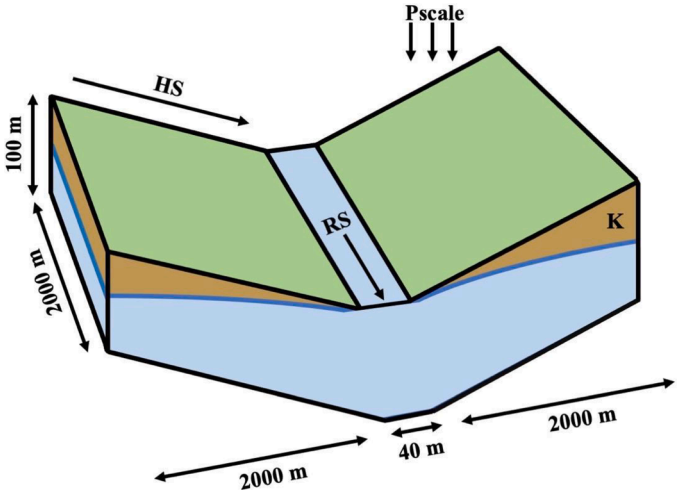

Fig. 1. A conceptual schematic of the idealized tilted-v domain of two hillslopes and river channel.

Slope (RS), was constant at 0.01. The subsurface was kept homogenous for this study, with the same subsurface properties used for both the channel and hillslope as has been implemented in previous tilted-v studies (S. Kollet et al., 2017; Rahman et al., 2019). Additionally, for all simulations, the porosity is 0.4 and the Van Genuchten parameters are alpha equal to 6 and n equal to 2. These additional parameters for the subsurface parameters can alter the domain's response; however, they were unchanged in this study.

2.2. Hydrologic Model and Boundary Conditions

All the simulations were run using the integrated physical hydrologic model ParFlow, which solves three-dimensional variably saturated groundwater flow and surface water flow. The subsurface is simulated with Richards Equation and overland flow is simulated using the two-dimensional kinematic wave equation. The details of ParFlow are provided in Ashby and Falgout (1996), Jones and Woodward (2001), S. J. Kollet and Maxwell (2006), and Reed M. Maxwell (2013). We chose to use an integrated hydrologic model because we want to explore the role of subsurface buffering on streamflow dynamics. Therefore, it is important to select a hydrologic model which simulates lateral groundwater flow and captures the dynamics of groundwater-surface water interactions. With ParFlow, there is a terrain following grid option which was implemented in this study with the assumption that our 100m domain is sufficiently deep for this configuration to not affect the results.

For our simulations, the surface boundary conditions of the tilted-v domain included is a free surface overland flow boundary condition. In the subsurface, no flow boundary conditions were implemented across the domain with the surface being the only outlet in the system. ParFlow fully integrates the groundwater surface water systems with a free surface overland flow boundary condition. This approach dynamically swaps to solving the overland flow equations when and wherever the pressure is greater than zero at the land surface. This boundary condition allowing groundwater-surface water interactions to evolve dynamically over the course of a simulation (i.e. for streams to form and disappear depending on saturation levels). Tilted-V domains similar to the one being used here have been thoroughly validated in previous model benchmarking and intercomparison studies (S. Kollet et al., 2017; Reed M. Maxwell et al., 2014), and are included in ParFlow's standard test suite.

2.3. Adjustable Parameters

The conditions outlined in Section 2.1 and Section 2.2 remained constant throughout this study and across all the simulations in the ensemble that was created. Three model parameters were adjusted as follows to better understand their influence of the power shift on the input precipitation signal;

1 Three hillslope (HS) values were used; 0.02, 0.05, and 0.08. These values are consistent with other hillslope or tilted-v studies (Bearup et al., 2016; Reed M. Maxwell, 2010; Mikkelson et al., 2013).
2 Hydraulic conductivity (K) values range from 0.5 to 15 m/day. This range was selected to span common literature values for K.
3 Five precipitation scalers (Pscale) were tested: 0.1, 0.25, 0.5, 0.75 and 1. Pscale values are applied by simply multiplying the entire precipitation time series by this value.

Our approach treats the precipitation signal as an approximately "white noise" input signal (the slope of the log-log periodogram for this signal is 0.12), and our goal is to study its evolution through the watershed. It should be noted that other processes like evapotranspiration and snowpack would also modify the input moisture signal to a watershed. For the purposes of this study, we don't consider this input signal variability though. We focus on the ways in which topography and geology transform a white noise input.

Our full ensemble includes 59 simulations and is outlined in Table 1. We test every Pscale and HS combination; however, we run transient simulations only for the K values that resulted in reasonable groundwater configurations in our initial spin up runs (i.e. water table depths with minimal ponding occurring outside the river, and where there was still sufficient water for a river to form).

2.4. Ensemble Spin-up Protocol and Transient Simulations

For each simulation, the following 'spin-up' protocol was followed to initialize the groundwater configuration. First, we run 100-year simulations with a daily time step and a constant precipitation forcing equal to the long-term average of precipitation to reach steady state groundwater configurations. Next, using the water table configurations from the steady state simulations as the initial condition, an additional 30-year transient spin up simulation was run with the first two years of the full precipitation time series being repeated 15 times, also with a daily timestep.

After the transient spin ups were complete 95-year transient simulations were run utilizing a historically based precipitation time series applied uniformly over the domain. Here too all simulations are completed with a daily timestep. The original precipitation time series is a 95-year daily record from rain gauge data from Fredonia, NY from the climate Data Online database through the NOAA National Centers for Environmental Information. This dataset was selected because it had a continuous record of rainfall measurements for a sufficiently long record. As previously discussed, the precipitation time series was altered by multiplicative factors of 0.1, 0.25, 0.5. 0.75. and 1. It is important to note that evapotranspiration was not modeled in this study as we used this precipitation time series to represent a white noise input signal.

2.5. Model output calculations: Streamflow, Storage, and Soil moisture

From the ParFlow model outputs, several time series and metrics were directly calculated from the ParFlow simulation gridded outputs of pressure and saturation. The methods for each of these calculations are outlined individually.

Streamflow: For each daily timestep of the transient simulations, the streamflow leaving the domain was calculated. Streamflow is the sum of any overland flow exiting the domain at any cell along the bottom edge (y = 0) with the overland flow formulation Eq. 1:

$$Q = \left(P^{5/3} * \frac{Sy}{\sqrt{\frac{1}{2}(Sx^2 + Sy^2)}} \right) \Big/ n * dx, \tag{1}$$

where Q is the daily streamflow (m^3/d), P is the ponded pressure head of

Table 1
Complete ensemble of simulations.

Slope of Hillslope (HS)	Precipitation Factor (Pscale)	Hydraulic Conductivity (m/d)
0.02	0.1	1, 1.5, 2, 5, 10
0.02	0.25	1, 1.5, 2, 5, 10
0.02	0.5	1.5, 2, 5, 10
0.02	0.75	2, 5, 10
0.02	1	5, 10
0.05	0.1	0.5, 1, 1.5, 2, 5
0.05	0.25	0.5, 1, 1.5, 2, 5
0.05	0.5	1, 1.5, 2, 5, 10
0.05	0.75	1, 1.5, 2, 5, 10
0.05	1	1.5, 2, 5, 10, 15
0.08	0.25	0.5, 1, 2, 5
0.08	0.5	0.5, 1, 1.5, 2, 5
0.08	0.75	1, 1.5, 2, 5, 10
0.08	1	1, 2, 5

the cell (m), Sx and Sy are the slopes in the x- and y- direction, n is manning's coefficient, and dx is the cell width in (m).

Storage: The total storage (m^3) of the domain was calculated at each timestep as the sum of subsurface storage, both saturated and unsaturated, as well as surface storage. Surface storage found by multiplying the cell area (dx * dy) by the pressure value for each cell with ponded water. For the subsurface storage the saturation was multiplied by the porosity (0.4) and then by the cell volume (dx * dy * dz) to find the volume of incompressible storage in each cell. Subsurface storage is divided into several components for analysis:

- Soil Moisture Storage: The storage in the top 2.5m of the domain (i.e., just the top layer). Note that this can include both saturated and unsaturated grid cells.
- Saturated Storage: The storage in cells with a saturation value of 1. The location of these cells may change over the course of the simulation as the subsurface drains and fills thus there is not constant spatial definition here.
- Unsaturated Storage: The storage in cells with saturation values less than 1.

Water Table Depth (WTD): For each simulation, the WTD was calculated for each timestep as the average distance from the surface to the water table for the entire domain. These values were then averaged across the time series of the whole simulation so that there is a single WTD value for each simulation.

2.6. Power Spectral Density

Power Spectral Densities (PSDs) and power spectra are established methods to explore the temporal scaling behavior of physical and chemical watershed signals. Previous researchers have applied spectral methods to analyze the temporal scaling behavior of streamflow (Gall et al., 2013; Guan et al., 2011; Pandey et al., 1998; Sauquet et al., 2008; Tessier et al., 1996), soil moisture (Amenu et al., 2005; D'Odorico & Rodríguez-Iturbe, 2000; Wu et al., 2002), water table depth (Condon & Maxwell, 2014), hydraulic head and groundwater well levels (Li & Zhang, 2007; Schilling & Zhang, 2012; Zhang & Li, 2005; Zhang & Schilling, 2004; Zhang & Yang, 2010), latent heat (Condon & Maxwell, 2014; Little & Bloomfield, 2010), chemical responses (C. J. Duffy & Gelhar, 1985; Christopher J. Duffy & Gelhar, 1986), chloride concentrations (Kirchner et al., 2000), and nitrogen concentrations (Zhang & Schilling, 2005).

Essentially this approach consists of a Fourier transform to shift time series to the frequency domain (as illustrated in Fig. 2). The power spectral density (PSD) represents the power of the signal present at each frequency and it squares the magnitude of a discrete Fourier transform. Higher values in the power spectrum indicate that a given frequency is contributing more to the variance in the signal.

There are numerous methods to estimate the PSD of a time series. Here, the PSD of the input (precipitation) and output (streamflow, unsaturated storage, and saturated storage) time series were generated utilizing the Scipy signal.periodogram function in Python and applied the "Hann" window. In order for the PSD to not be a function of the size of the storage values, the PSDs were normalized by the maximum PSD value so that each periodogram had a range of 0 to 1; however, we did not normalize the areas under the curves.

2.7. Transfer functions

Transfer functions (TF) are a method to quantify the differences between two power spectral densities. Here we use this method to explore shifts in the temporal dynamics between the input precipitation signal and the simulated streamflow. Transfer functions have been applied in hydrologic context to analytical solutions of aquifer models of varying complexity (Gelhar, 1974; Russian et al., 2013) and have also been used for parameter estimation (Pedretti et al., 2016). Traditionally, transfer functions are derived from stationary linear systems. This is of course not true for hydrologic systems. However, our goal is not to derive transfer functions that can fully describe the system. Rather, we are simply using the transfer function as a method to investigate the controls of signal filtering. Our method of calculating transfer functions from the input PSD and output PSD is consistent with Pedretti et al. (2016) and Schuite et al. (2019).The transfer function is calculated as the ratio of the PSD of the output signal to the input signal (Pedretti et al., 2016; Schuite et al., 2019) as in Eq. 2:

$$TF = \frac{PSD_{output}}{PSD_{input}}, \tag{2}$$

where the output is the streamflow PSD, and the input is the precipitation PSD for the same frequency range. Here the Transfer Function is first calculated across all frequencies in the PSDs and is then smoothed using a simple moving average following the approach of (Schuite et al., 2019). Here we also average the TF across specific period windows of interest (3-14d, 14d-3m, 3m-1y, 1-5y, 5-10y, 10-30y) to provide summary metrics of high and low frequency damping.

2.8. Soil Moisture and Total Storage Memory

In addition to spectral methods which can provide information about individual timescales of variability, memory metrics can provide an

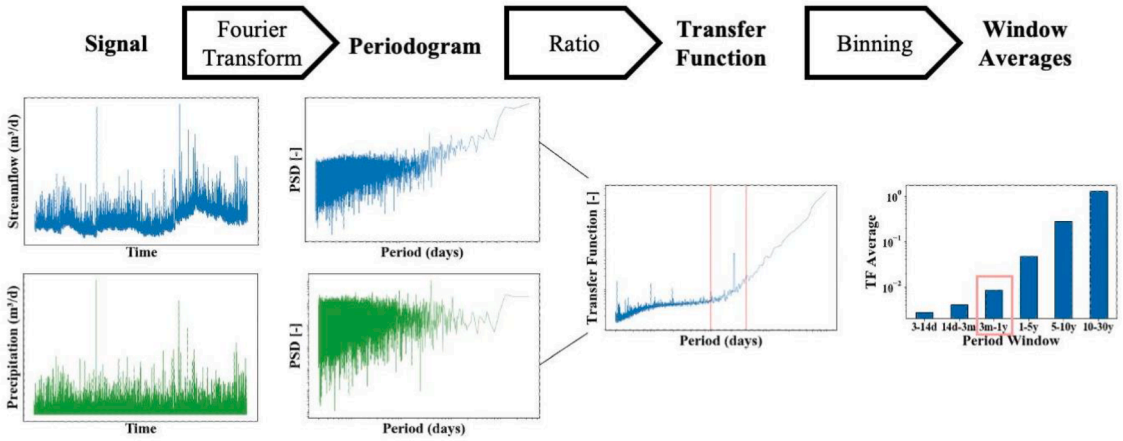

Fig. 2. Conceptual workflow of how the periodograms, transfer function, and transfer function averages were calculated from the streamflow and precipitation signals. The red lines on the transfer function show the range of the window averaged for finding the boxed value in the bar plot.

intuitive way to quantify overall signal persistence. The memory of a hydrologic variable is generally a measure of how that variable is likely to evolve in time and the timescale at which an anomaly is likely to persist. There are many ways to calculate memory; for example, calculating the time needed for an anomaly to dissipate using an autocorrelation calculation, finding the mean persistence time or length of time the value spends over a certain threshold, or calculating remaining precipitation fractions (F_P).

For this study, the surface storage, total storage, and soil moisture storage memory were evaluated by calculating the fraction of precipitation anomalies (F_P) that remain after a given time lag as presented by McColl et al. (2017). More specifically, the remaining precipitation fraction is defined as the ratio of positive changes for a given storage time series (e.g., soil moisture) divided by the total amount of precipitation. In this study, F_P was calculated for the time series of both soil moisture storage and total storage. For a given time series (f), the calculation for F_P is found using Eq. 3 for a storage moisture time series (θ) with T timesteps (days):

$$F_P(f) = \frac{\sum_{i=1}^{fT} \Delta\theta_{i+}}{\int_0^T P(t)dt}, \quad (3)$$

where $\Delta\theta_{i+}$ is the positive change in the soil moisture ($\Delta\theta_{i+} = 0$when there is no change or a negative change in storage), dt is the frequency of the time series (1 once per day), and the denominator is the total precipitation across the domain for the entire time series. The sampling frequency (or time lag), i, was altered by changing the number of days between the positive changes in soil moisture. Note that F_P is dependent on the frequency that the time series is sampled, which corresponds to the time lag that is being evaluated (i.e., the value of i). Here we calculate F_P over a range of memory sampling frequencies (or time lags) to explore how much of the signal is left at various time scales. F_P was calculated at the sampling frequencies of 1, 2, 3, 5, 7, 10, 14, 30, 60, and 90 day(s). For a memory sampling frequency of 1 day the $\Delta\theta_{i+}$ is calculated between each day whereas for a memory sampling frequency of 7 days the $\Delta\theta_{i+}$ value would only be calculated each 7 days.

We selected this approach based on the findings of (McColl et al., 2017) who compared the F_P method to various other memory metrics and demonstrated that many of the historically used methods, such as autocorrelations with fixed time lag, overestimate soil moisture memory. Additionally, we could readily apply the remaining precipitation fraction method to other time series other than soil moisture such as total storage.

3. Results

3.1. General trends

Three representative cases are selected in Fig. 3 to illustrate a range of response behaviors in the surface and subsurface for a given precipitation input. For every simulation in Fig. 3, there are increases in structure and reddening of the signal from the initial noisy precipitation input moving through the domain from streamflow to soil moisture, unsaturated storage, and finally saturated storage. This illustrates the increased filtering that occurs with depth as signals move through the subsurface and more energy is removed. In all three of the saturated storage signals shown in Fig. 3, hourly and daily variability is almost entirely absent.

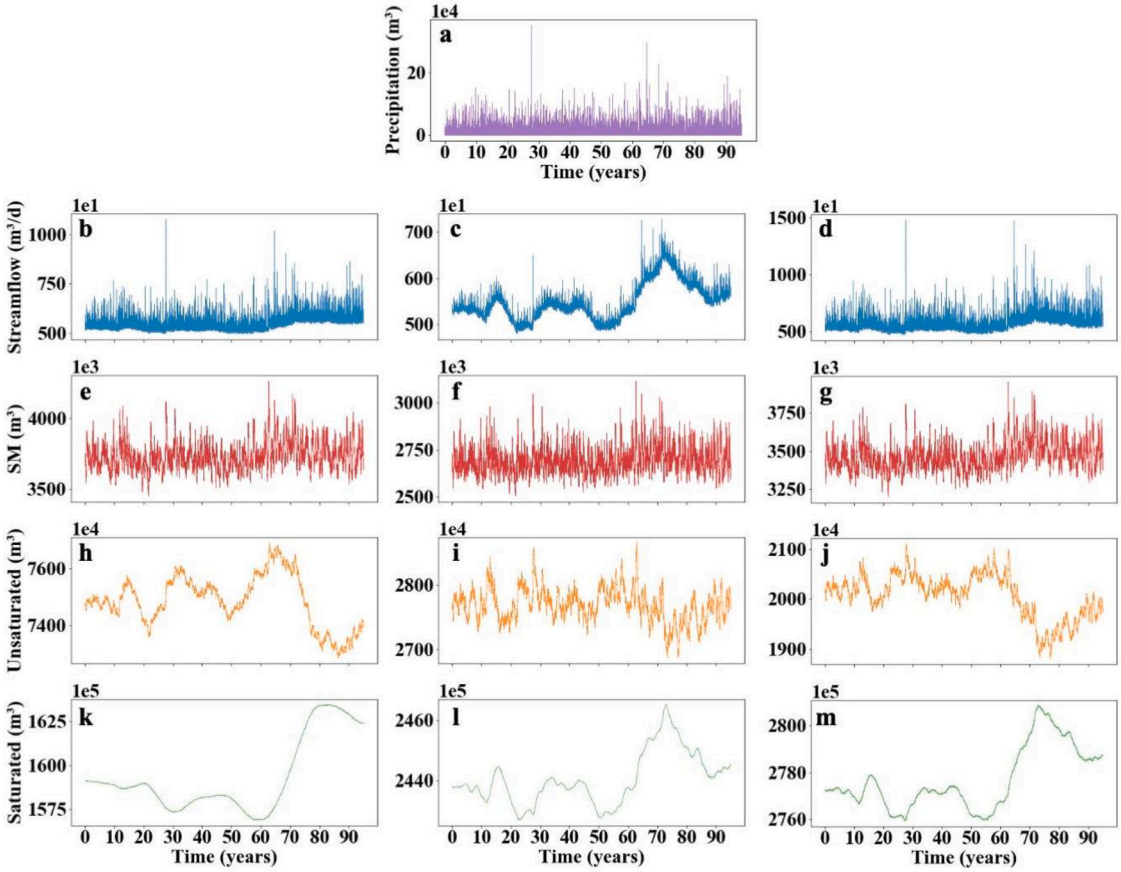

Fig. 3. a) Precipitation input time series for the three selected simulations with Pscale equal to 0.25. The output time series include b-d) streamflow, e-g) soil moisture, h-j) unsaturated storage, and k-m) saturated storage for three simulations with varying K and HS values and the same Pscale value of 0.25 (left column: K = 0.5, HS = 0.08, middle column: K = 10, HS = 0.02, right column: K = 1.5 HS = 0.02).

The difference between the cases (i.e., columns) shown in Fig. 3 highlight the impact of watershed characteristics on the filtering process. The left (b, e, h, k) simulation has the lowest K value in Fig. 3, which causes the most energy to be removed in the subsurface and by the time the signal has reached the saturated storage the high frequency components of the input signal have been removed and results in the smoothest unsaturated and saturated storage signal. Additionally, with this lower K value we would expect this system to be the most stable and which can be observed as there is an observed attenuation in the peak value between 60 and 80 years.

The center (c, f, i, l) and right (c, g, j, m) simulations are flatter and drier than the first column and both have HS values of 0.02 (relative to the first case with HS=0.08). The right and left simulations of streamflow signals are similar; however, have very different subsurface signals. The only difference between the center and right cases are their K values. The center simulation has a high K value resulting in a very responsive streamflow signal whereas the right simulation has a more stable streamflow baseline with larger daily peaks from larger overland flow events. When comparing the saturated storages, both the center and right simulations have higher K values and therefore have more variability in the storage signals less energy is lost as it moves through the subsurface. The raw time series of these select simulations illustrates qualitatively the impact that watershed properties can have on the degree of filtering and how it varies with depth.

To evaluate ensemble characteristics more quantitatively, the memory of soil moisture, surface storage, unsaturated storage, and saturated storage were all calculated using the fraction of precipitation (F_P) (McColl et al., 2017) at various sampling frequencies. As the sampling frequency decreases (i.e., the time scales increase) the memory intuitively decreases (consistent with the idea that signals are dampened out over time). The ranges of F_P for each sampling frequency across the entire ensemble of simulations are plotted in Fig. 4. The surface storage is the smallest storage body with the fastest response times; its F_P values are significantly smaller than the other parts of the system and decay to zero much more quickly.

The subsurface storages (unsaturated, saturated, and soil moisture) all have larger values for daily sampling frequencies and maintain memory much longer than the surface system. Memory is calculated based on the precipitation signal, the unsaturated zone responds most quickly to this signal and has the greatest memory due to the long-term correlation with the precipitation signal. The soil moisture is the top 2.5m of the domain and can contain both saturated and unsaturated cells and therefore is in-between the saturated and unsaturated storage memories. The saturated storage memory drops off more quickly and is lower than the unsaturated and soil moisture memories. This is consistent with Fig. 3 where we demonstrate significant dampening in the saturated storage component of the system. Also, due to the larger role of lateral redistribution that happens with the saturate storage (flow in the unsaturated zone is primarily vertical) we expect for the direct correlation to precipitation to be weaker in this component of the system.

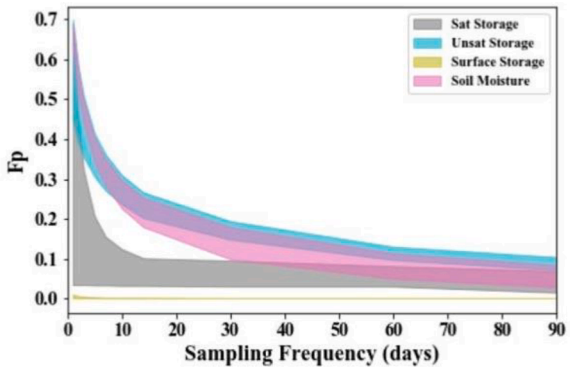

Fig. 4. The range of F_P values for soil moisture, unsaturated storage, saturated storage, and surface storage for sampling frequencies between 1 and 90 days.

3.2. Connection between watershed properties and degree of filtering

Next, we explore how watershed properties affect the temporal filtering properties using transfer functions. As described in the methods section, we are presenting the average transfer functions over a preselected set of time periods for streamflow, unsaturated storage, and saturated storage. It is important to note that in these results, transfer functions are used as a method to understand the signal transformation of the input signal that takes place. Transfer function values greater than one indicate a shift in power or signal transformation whereas transfer function less than one indicate filtering has occurred. As is consistent with the analysis of Schuite et al. (2019), we showed that the cumulative power spectrum for streamflow is expected to asymptote at a value of one but other variables, in our case saturated and unsaturated storage, approach values greater than one. Base on previous studies such as Yang et al. (2018), filtering and memory increase as we move deeper into the subsurface. As such, relative to streamflow we expect a larger proportion of groundwater signal to be in the longer periods.

Fig. 5 shows the average transfer function (i.e., portion of the signal that is maintained) for the entire time series. The values are colored by the ratio of the Pscale over K. This ratio was chosen because it reflects the degree of partitioning between runoff and infiltration. Recall the larger transfer functions indicate that less filtering has occurred, and smaller transfer function values indicate more filtering or signal transformation has occurred. For streamflow (Fig. 5a) steeper hillslopes lead to deeper WTD, which in turn correlates to a larger unsaturated zone buffer, and greater filtering. Fig. 5a shows three distinct curves depending on the slope of the watershed that illustrate this relationship. For a given water table depth steeper slopes result in less filtering. Additionally, larger Pscale over K ratios lead to more runoff (and smaller values leading to more infiltration). Thus, as the Pscale over K ratio increases (darker colors in Fig. 5a) there is less filtering due to more of the precipitation generating runoff rather than infiltrating.

Conversely, for unsaturated storage (Fig. 5b) these relationships are flipped. Here there is a slight positive relationship between WTD and transfer function values (indicating less filtering with deeper water table depths). This relationship is much weaker than what was observed for streamflow though. Also, we see a positive relationship between the Pscale ratio and filtering (i.e., less filtering when the Pscale over K ratio is smaller). This makes sense as precipitation partitioning will shift toward infiltration as the Pscale over K ratio decreases leading to greater infiltration and a noisier signal in the subsurface.

Finally, for saturated storage (Fig. 5c) the degree of filtering is much greater than unsaturated or streamflow components (roughly an order of magnitude higher as can be seen from the x-axis ranges). This is consistent with Fig. 3 that illustrated the significant filtering of the storage signal. Interestingly, we do not see a relation to WTD for saturated storage. Once again, the Pscale over K ratio color gradient shows that as the ratio increases, the filtering increases which is once again due to increasing infiltration as the ratio decreases.

To further investigate the controls of the filtering at different temporal scales, the transfer functions for each metric are binned and averaged over periods of interest. Fig. 6 shows the degree of filtering at six different period windows for the streamflow signals of the entire ensemble. For streamflow less than ~5 years (Fig. 6a-d), there is a direct relation between WTD and the amount of filtering that we see; deeper water tables lead to more filtering (smaller transfer function values) and shallower water tables lead to less filtering. Furthermore, at these periods less than 5 years, as the Pscale to K ratio increases there is also a decrease in the amount of filtering. This indicates that configurations with higher precipitation and lower K values have less filtering occurring and is consistent with increased runoff partitioning for infiltration excess overland flow when precipitation exceeds the infiltration rate

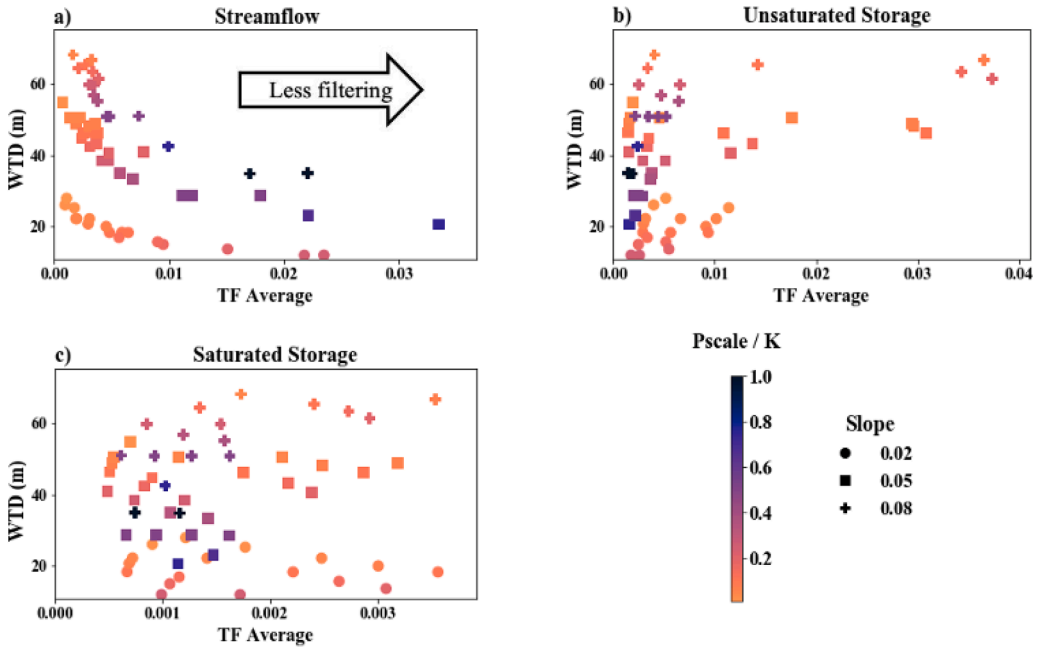

Fig. 5. The average WTD (m) is plotted versus the average transfer function for every simulation for a) streamflow b) unsaturated storage c) saturated storage. The shape indicates slope, and the color indicates the Pscale to K ratio.

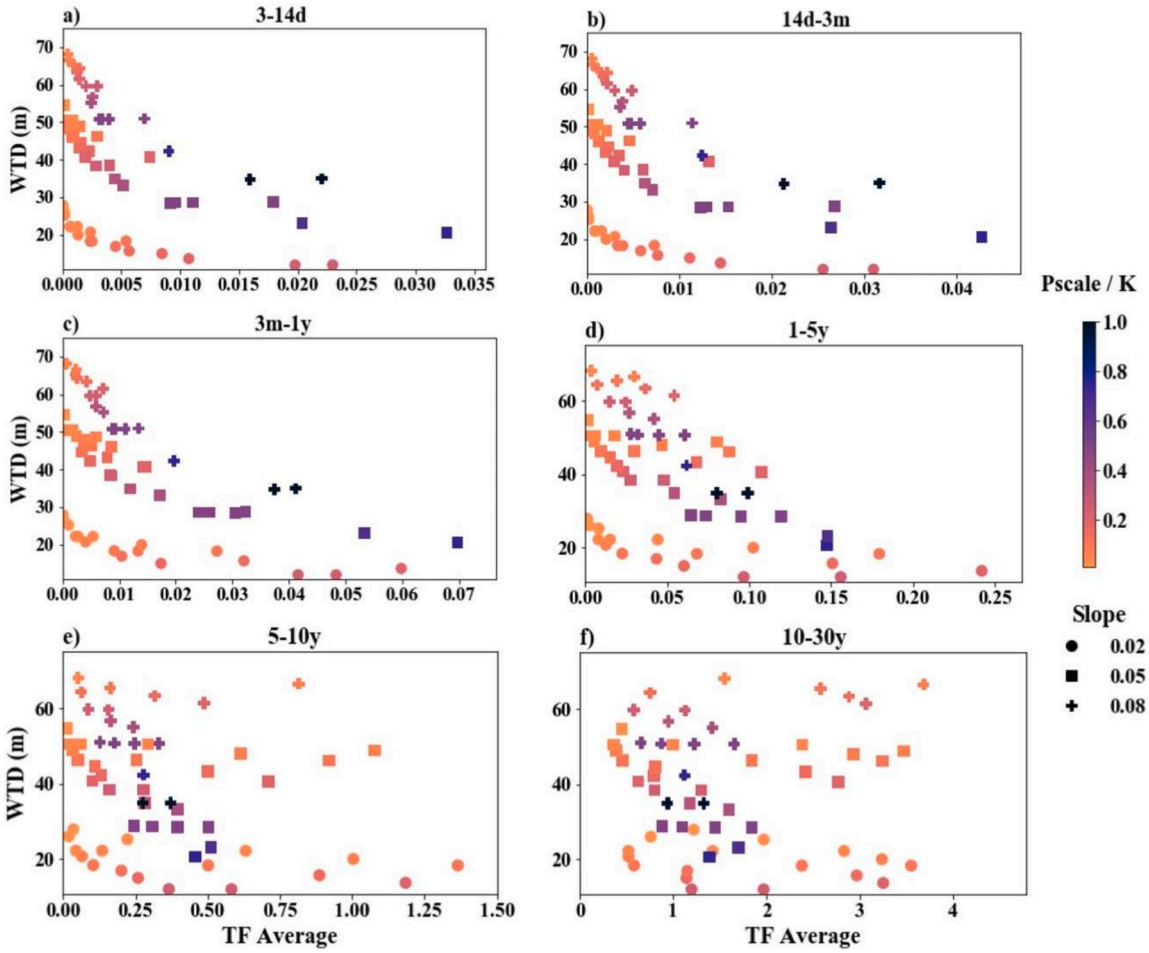

Fig. 6. The average streamflow transfer function values versus the average WTD across six period windows a) 3-14d, b) 14d-3m, c) 3m-1y, d) 1-5y, e) 5-10y, f) 10-30y. The color indicates the Pscale: K ratio and the shape indicates the hillslope.

controlled by K. For longer periods (greater than 5 years), the relationship between water table depth and degree of signal transformation is less clear. Note, that the TF values especially for the periods over 10 years for are often greater than one, indicating the power shift rather than true filtering taking place. At these longer timescales, there is stronger connection to precipitation here with higher precipitation correlating to less filtering (i.e., a noisier streamflow signal).

The same period windows are used in Fig. 7 for the unsaturated storage transfer function averages; however, the points are shaded by their K values (as opposed to the Pscale/K ratio) because stronger relationships were found for K in this part of the system. For the shorter periods, less than 3 months (Fig. 7a, b), there is significant filtering, and a very small portion of the original signal remains (less than 1%). Nearly all the power at these periods is removed from the signal as it is filtered through the subsurface. Generally, for all period windows, filtering decreases (i.e., transfer function values increase) as K increases. This makes sense because higher K values allow for greater infiltration and for the signal to transfer more quickly through the subsurface.

Looking at the periods greater than 3 months, there is still a positive inverse relationship between K and the degree of filtering or signal transformation taking place. As with the previous plots, steeper slopes lead to deeper water tables. There is not a clear relationship between water table depth and filtering for periods less than one year. However, for a given water table, higher K values result in less filtering. For the longest periods (Fig. 7d, e, f) we can again see distinct trends emerging between water table depth and degree of signal transformation for a given slope value. The deeper the water table leads to greater TF values. This seems counterintuitive as we would expect to see greater filtering with depth; however, WTD is also a function of K and indeed we see a positive correlation in the coloring with higher K values for the deeper WTD of a given slope. Here we are likely seeing the nonlinear impacts of increasing K in the unsaturated zone, which is controlling the signal transformation and filtering.

Finally, Fig. 8 shows the degree of filtering or the power shift taking place over the six period windows for the saturated storage component of the domain. Similar to the unsaturated storage in Fig. 7, the shorter periods experience significant filtering and nearly all the power at these periods is removed from the signal (less than 1% remains). However, since the signal must move through more of the subsurface before reaching the saturated storage, and given the dampening impacts of lateral flow, even more filtering and damping occurs. For this reason, the saturated transfer function values are smaller than the unsaturated storage value at all time scales and the periods of significant damping includes all periods less than 1 year (Fig. 8 a-c, note that for unsaturated storage this was only up to 3 months).

Focusing on the relationships for periods greater than 1 year, once again the filtering is inversely correlated to the K values. Simulations with the high K values exhibit the least filtering across all periods in the saturated storage. Once again, the slopes are still positively correlated to the WTD and for a given WTD, the K value determines the degree of filtering. Interestingly though, for a given slope and K value (e.g., the red squares or the purple dots in Fig. 8e, f) we now see an inverse relationship between WTD and TF indicating more filtering or more of a transformation with deeper water table depths. This is consistent with the idea of increased filtering and more of a power shift in the subsurface with depth. As noted above we hypothesize that the nonlinear relationship between saturation and hydraulic conductivity in the unsaturated zone increases the relative importance of K leading to decreased

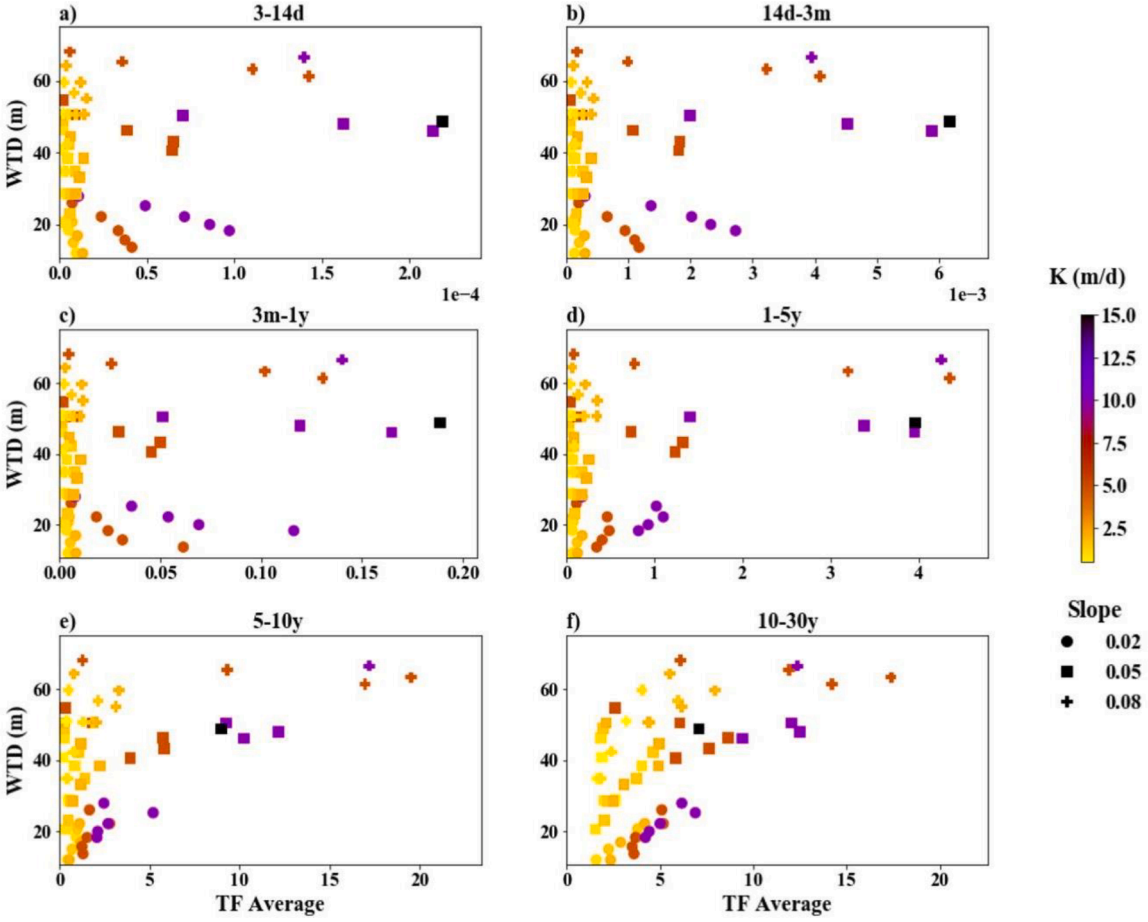

Fig. 7. The average unsaturated storage transfer function values versus the average WTD across six period windows a) 3-14d, b) 14d-3m, c) 3m-1y, d) 1-5y, e) 5-10y, f) 10-30y. The color indicates the K (m/d) values, and the shape indicates the hillslope.

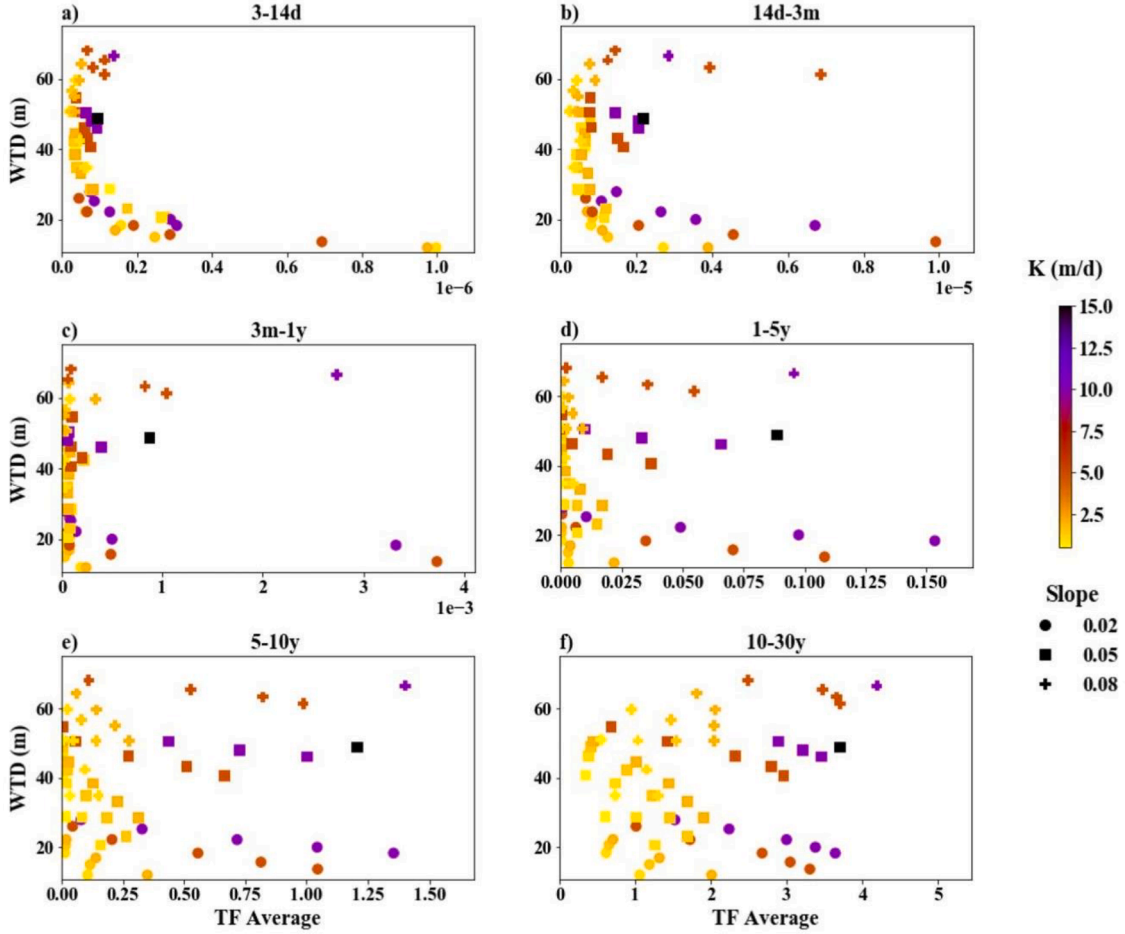

Fig. 8. The average saturated storage transfer function values versus the average WTD across six period windows a) 3-14d, b) 14d-3m, c) 3m-1y, d) 1-5y, e) 5-10y, f) 10-30y. The color indicates the K values, and the shape indicates the hillslope.

filtering with increased depths.

Figs. 6-8, show the controls of the filtering and signal transformations for the entire ensemble. To further illustrate how the watershed parameters affect the signal transformation behavior, representative cross sections of the ensemble were selected where only a single variable is altered. In Fig. 9, only the K values change over an order of magnitude as the Pscale and HS values are held constant. For the streamflow (Fig. 9a), higher K values lead to more filtering, with the strongest relationship occurring for periods less than 5 years. For the longest period (10-30y), this relation flips and higher K values lead to less filtering for periods 10-30 years. Conversely for both unsaturated storage (Fig. 9b) and saturated storage (Fig. 9c), the relation is consistent across nearly all periods with higher K values leading to higher TF values. These findings are consistent with what was discussed in Figs. 7 and 8, and the basic physical controls of these system components. At the land surface higher K values lead to more infiltration, less overland flow and a larger baseflow component (i.e., greater filtering). Whereas in the subsurface the K value controls the flux rates.

Fig. 10 shows a different cross section where the K and HS values are held constant and the Pscale values change. As shown here, both streamflow and saturated storage have inverse relations between the amount of precipitation and filtering. As the precipitation increases, there is less filtering (larger transfer function) across all the scales and for all Pscale values. Interestingly, for unsaturated storage (Fig. 10b) this is true for Pscale values < 0.5, after which the trend reverses and there is actually more filtering for larger Pscale values. For HS, there was a larger variety of trends across the cross sections of the full ensemble and a single representative trend was not possible.

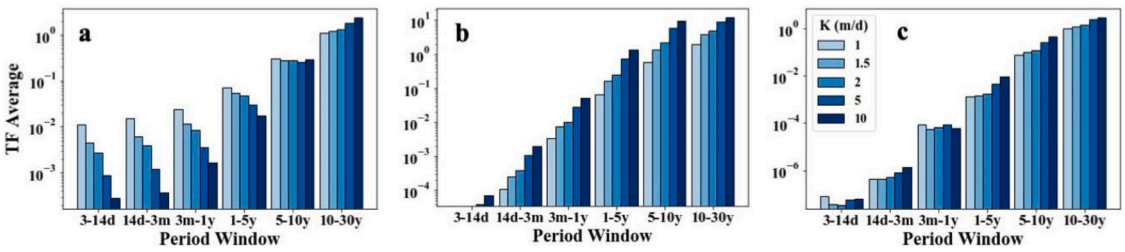

Fig. 9. The average transfer function values for representative K ensembles across six period windows on a log scale for a) streamflow, b) unsaturated storage, c) saturated storage. The color indicates the K value with darker blues indicating higher K values.

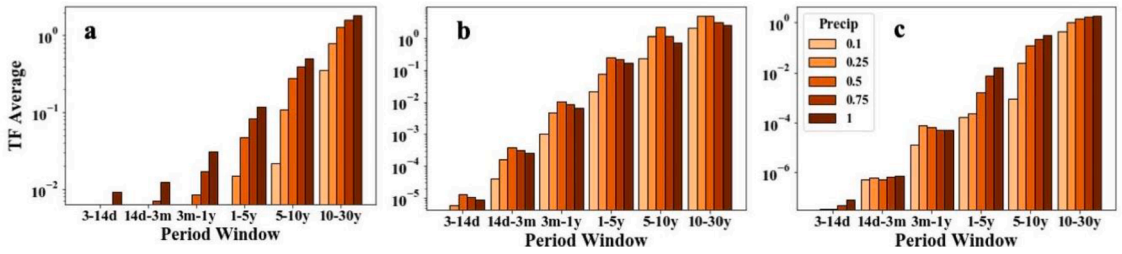

Fig. 10. The average transfer function values for representative precipitation ensembles across six period windows on a log scale for a) streamflow, b) unsaturated storage, c) saturated storage. The color indicates the K value with darker oranges indicating higher Pscale values.

4. Discussion

Previous research has demonstrated that filtering and damping of the precipitation signal increases moving deeper into the subsurface (Li & Zhang, 2007; Yang et al., 2018). Here we explore the way that watershed characteristics control the degree of signal transformation moving from streamflow to unsaturated and saturated storage through a series of controlled numerical experiments. It should be noted that the storages which we investigated are not independent variables and the dynamics of saturated storage depends on infiltration, recharge, and baseflow. Our goal in this study is not to fully attribute all sources of variability, but rather to understand the interactions between subsurface storage dynamics and streamflow.

In order to achieve well controlled numerical experiments, numerous simplifications were made in our models. First, we used a real-world precipitation and with this input signal all of the precipitation adjustments are scalers. We did not explore changing precipitation variability and instead focus on the ways in which topography and geology transform a white noise input. However, changes in the temporal distribution of rainfall events and not just their magnitude would alter the driving frequencies of the domain and could influence our results. We also assumed a homogenous and idealized domain to limit the topographic and hydrogeologic complexity. More complex watersheds configurations would impart additional temporal structure through the close interactions between groundwater configuration, geology and topography.

We also excluded evapotranspiration from our simulations, this could also be spatially variably depending on land cover type. However, we recognize that evapotranspiration is an important hydrologic control especially for real-world studies. Furthermore, these simulations were run at a daily scale so that we could run sufficiently long simulations to analyze the long-term trends; however, running at this temporal resolution limits our ability to analyze short-term phenomena like pressure propagation. Finally, the baseline configuration and boundary conditions, and resolutions also are considerations that would alter the results. As stated in the Methods (Section 2.2), no-flow boundary conditions were set in the subsurface. Using these boundary conditions, our water tables might be shallower than if another boundary condition was used and then alter the streamflow responses of the simulations. Furthermore, in this study, some of the lowest WTD simulations resulted

Table 2
A conceptual table to indicate how each variable controls the observed filtering or signal transformation behavior of the watershed. Blue up arrows indicate that as the variable increases the degree of filtering/transformation will increase. Red down arrows indicate that as the variable increases the degree of filtering/transformation will decrease. Key variable controls are highlighted by the bold arrows.

	Short Term Controls	**Long Terms Controls**
Streamflow	Periods (3d-5y) WTD: **↑** K: ↑ Pscale: ↓ Pscale/K: **↓** Slope: ↑	Periods (5-30y) WTD: --- K: **↓** Pscale: **↓** Pscale/K: --- Slope: ---
Unsaturated Storage	Periods (3d-3m) Most of signal removed	Periods (3m-30y) WTD: **↓** K: **↓** Pscale: --- Pscale/K: **↑** Slope: **↓**
Saturated Storage	Periods (3d-1y) Most of signal removed	Periods (1-30y) WTD: **↑** K: **↓** Pscale: **↓** Pscale/K: --- Slope: ---

in considerable excess ponding outside of the river channels. One area where excess ponding could affect our results is in the Fp of saturated memory. The ensemble member with the highest Saturated Storage Fp at the daily scale had considerable ponding, without this member or runs with similar ponding we'd expect the range of Saturated Storage Fp to be reduced.

Even in this relatively simple system the range of controls is complex and varies by the temporal scale. Looking at individual parameters (K, Pscale, or HS) can sometimes explain the filtering behaviors and signal transformations of the system, but a combination of these parameters better encapsulates the physical processes at work such as WTD or Pscale/K. Table 2 provides a conceptual summary of the short-term and long-term signal transformation and filtering controls based on the results in Figs. 6-8.

For streamflow, the filtering controls vary depending on the period length. For short periods (3d-5y), we show that as the WTD increases, the degree of filtering increases. This is consistent with a deeper and more filtered baseflow component with deeper water table depths. The other key control for these periods is the Pscale/K ratio, which determines the amount of infiltration versus overland flow we would expect to see. With higher Pscale/K values, there is more overland flow and less infiltration, leading to less filtering (Fig. 6).

For longer-term streamflow filtering (greater than 5 years), WTD and Pscale/K ratio are no longer the key controls of filtering. Rather, here we see a positive relationship between filtering and K. Indicating that it is instead how readily the precipitation signal can propagate through the surface that controls the degree of filtering. Higher K values allow for less energy to be lost in the subsurface and less filtering of the precipitation signal. Furthermore, we see less filtering with the higher Pscale values as the increased precipitation leads to larger gradients in the subsurface which maintain more of the signal. The changes in relationship seen with longer time scales are likely due to the increased importance of baseflow dynamics in determining low frequency streamflow variability.

The increased filtering behavior at shorter timescales is consistent with the findings of Li and Zhang (2007). They looked at how the scaling of different hydrological signals (rainfall, streamflow, groundwater, baseflow) compared and then also analyzed how they changed at different timescales. They similarly found that the scaling increased as the subsurface buffer increased and that this trend could be attributed to the dampening of the signal. Additionally, they found that the scaling decreases at longer timescales. While they considered significantly smaller time scales (less than 1 year) and did not directly analyze the unsaturated zone, the general findings are consistent with our results.

For both saturated and unsaturated storage nearly all of the signal is removed for the shortest periods (3d-3m). This agrees with previous findings of (Yang et al., 2018), that the greatest signal filtering occurs in the unsaturated zone. At the longer scales, K and Slope appear to be the primary controls. This is consistent with the drivers of infiltration. K determines the amount of energy lost as water passes through the subsurface. Furthermore, the impact of K can be amplified in the unsaturated zone where K varies nonlinearly as a function of saturation. HS has an inverse relation with the degree of filtering as steeper slopes lead to higher gradients. The primary role of K and HS in the unsaturated zone indicates that filtering here is a function of how quickly the signal moves through the subsurface. Increased K and steeper gradients both allow the signal to move more quickly and experience less filtering.

Perhaps counterintuitively though it should be noted that higher K's are also correlated with deeper water table depths, and therefore a deeper (thicker) unsaturated zone. We also find decreased filtering with increased water table depth in this part of the system. This would seem to contradict the logic of more filtering happening with more time spent in the subsurface as you move deeper. We hypothesize that this relationship occurs because the nonlinear relationship between K and saturation has a stronger impact on the filtering than WTD. Close inspection of Fig. 7 shows that for a constant K and slope values there is actually more filtering with deeper water tables.

Similar to unsaturated storage, saturated storage also exhibits nearly complete filtering for short time periods which was expected as it is well established that there is increased filtering with depth. An important difference for saturated storage is that the periods of nearly complete filtering extend further to 3d-1y. Once again in the subsurface K is a key control and as K increases less energy is lost and the signal can more readily move through the subsurface and less filtering occurs. For saturated storage, neither WTD, Pscale/K, nor HS have a strong influence on the signal filtering, but Pscale does have some influence. Unlike the unsaturated storage, the deeper WTD of the same K shows more filtering for saturated storage as was shown in Fig. 8. As for Pscale, as it increases the system is transmitting more water and the larger fluxes lead to larger gradients which in turn leads to high velocities and more noise can make it through the system. Like the unsaturated storage, it seems the WTD is not as important as the time spent in the subsurface.

5. Conclusions

In this study, the temporal dynamics of streamflow, soil moisture and groundwater storage are simulated with an integrated hydrologic model and through the use of spectral methods, the degree of filtering and signal transformation and how the transformation evolves in time is examined and trends at the short- and long-term timescales. Consistent with previous work we see persistent damping and attenuation as precipitation moves through the watershed – with the largest filtering occurring in the deepest parts of the subsurface, especially at the higher frequencies. Our work extends beyond previous studies to evaluate the connection between watershed characteristics and temporal filtering across times scales and at different parts of the system. Overall, we show that filtering and power shift between frequencies is controlled by the amount of time spent in the subsurface and the degree of groundwater surface water exchanges.

For the streamflow signal, the short-term and long-term controls vary by time period and represent the two different streamflow generation mechanisms, runoff and baseflow. For short periods, the primary controls of filtering are those most closely linked to runoff generation (i.e., Pscale/K ratio and WTD which can influence infiltration excess and saturation excess overland flow). At longer periods, the signal transformation is more strongly correlated to variables that control baseflow. We found that the higher K and higher Pscale values causes less filtering: higher K values lead to faster signal transmission in the subsurface and larger Pscale values increase the amplitude of the total signal in the subsurface.

In the subsurface, we found that both the saturated and unsaturated zones have significant filtering at the shorter timescales, and nearly all the high frequency variability is removed. Additionally, across all time scales K was the primary control of the subsurface filtering; however, there were some differences between the saturated and unsaturated zone and their filtering responses to Pscale and WTD. Specifically, there is more filtering in the saturated zone and for a wider range of timescales. Furthermore, the two storages show different signal transformation responses to WTD with unsaturated storage showing less filtering for deeper WTD and saturated storages showing more filtering for increases in WTD.

This work highlights the complexity of temporal filtering and signal transformations across hydrologic systems. We demonstrate differences in the physical controls across time scales and consider different components of the system. Additional studies looking at a wider range of watershed variables and their influence on filtering is needed for a better understanding on how hydrologic variables control signal filtering. This study attempts to minimize the complexities of the hydrologic system with an idealized watershed. In order to learn about the controls in real world watersheds, these analyses should be applied to more complex and differing watersheds. Finally, this research did not implement particle tracking software. Coupling similar research to particle tracking

could provide additional information about how these watershed variables alter the filtering ability of the subsurface.

CRediT authorship contribution statement

Abram Farley: Software, Formal analysis, Investigation, Data curation, Visualization, Writing – original draft. **Laura E. Condon:** Conceptualization, Methodology, Writing – review & editing, Supervision, Project administration, Funding acquisition.

Declaration of Competing Interest

The authors declare that they have no known competing financial interests or personal relationships that could have appeared to influence the work reported in this paper.

Data availability

Data will be made available on request.

Acknowledgements

The National Science Foundation (NSF) award number 1835794 supported this research. Additionally, all of the simulations and model runs were completed on the University of Arizona's High-Performance Computing (UAHPC) resources.

References

Amenu, G.G., Kumar, P., Liang, X.-Z., 2005. Interannual Variability of Deep-Layer Hydrologic Memory and Mechanisms of Its Influence on Surface Energy Fluxes. Journal of Climate 18 (23), 5024–5045. https://doi.org/10.1175/JCLI3590.1.

Ashby, S.F., Falgout, R.D., 1996. A Parallel Multigrid Preconditioned Conjugate Gradient Algorithm for Groundwater Flow Simulations. Nucl. Sci. Eng. 124 (1), 145–159. https://doi.org/10.13182/NSE96-A24230.

Bearup, L.A., Maxwell, R.M., McCray, J.E., 2016. Hillslope response to insect-induced land-cover change: an integrated model of end-member mixing. Ecohydrology 9 (2), 195–203. https://onlinelibrary.wiley.com/doi/abs/10.1002/eco.1729.

Carlier, C., Wirth, S., Cochand, F., Hunkeler, D., Brunner, P., 2018. Exploring Geological and Topographical Controls on Low Flows with Hydrogeological Models. Groundwater 57.

Condon, L.E., Maxwell, R.M., 2014. Groundwater-fed irrigation impacts spatially distributed temporal scaling behavior of the natural system: a spatio-temporal framework for understanding water management impacts. Environ. Res. Lett. 9 (3), 034009 https://doi.org/10.1088/1748-9326/9/3/034009.

D'Odorico, P., Rodríguez-Iturbe, I., 2000. Space-time self-organization of mesoscale rainfall and soil moisture. Adv. Water Res. 23 (4), 349–357. http://www.sciencedirect.com/science/article/pii/S0309170899000305.

Delworth, T.L., Manabe, S., 1988. The Influence of Potential Evaporation on the Variabilities of Simulated Soil Wetness and Climate. Journal of Climate 1 (5), 523–547. https://journals.ametsoc.org/doi/abs/10.1175/1520-0442%281988%29001%3C0523%3ATIOPEO%3E2.0.CO%3B2.

Duffy, C.J., Gelhar, L.W., 1985. A Frequency Domain Approach to Water Quality Modeling in Groundwater: Theory. Water Resour. Res. 21 (8), 1175–1184. https://agupubs.onlinelibrary.wiley.com/doi/abs/10.1029/WR021i008p01175.

Duffy, C.J., Gelhar, L.W., 1986. A Frequency Domain Analysis of Groundwater Quality Fluctuations: Interpretation of Field Data. Water Resour. Res. 22 (7), 1115–1128. https://agupubs.onlinelibrary.wiley.com/doi/abs/10.1029/WR022i007p01115.

Entin, J.K., Robock, A., Vinnikov, K.Y., Hollinger, S.E., Liu, S., Namkhai, A., 2000. Temporal and spatial scales of observed soil moisture variations in the extratropics. Journal of Geophysical Research: Atmospheres 105 (D9), 11865–11877. https://agupubs.onlinelibrary.wiley.com/doi/abs/10.1029/2000JD900051.

Freeze, R.A., Witherspoon, P.A., 1967. Theoretical analysis of regional groundwater flow: 2. Effect of water-table configuration and subsurface permeability variation. Water Resour. Res. 3 (2), 623–634. https://agupubs.onlinelibrary.wiley.com/doi/abs/10.1029/WR003i002p00623.

Gall, H.E., Park, J., Harman, C.J., Jawitz, J.W., Rao, P.S.C., 2013. Landscape filtering of hydrologic and biogeochemical responses in managed catchments. Landscape Ecology 28 (4), 651–664. https://doi.org/10.1007/s10980-012-9829-x.

Gelhar, L.W., 1974. Stochastic analysis of phreatic aquifers. Water Resour. Res. 10 (3), 539–545. https://agupubs.onlinelibrary.wiley.com/doi/abs/10.1029/WR010i003p00539.

Gleeson, T., Manning, A.H., 2008. Regional groundwater flow in mountainous terrain: Three-dimensional simulations of topographic and hydrogeologic controls. Water Resour. Res. (10), 44. https://agupubs.onlinelibrary.wiley.com/doi/abs/10.1029/2008WR006848.

Gleeson, T., Marklund, L., Smith, L., Manning, A.H., 2011. Classifying the water table at regional to continental scales. Geophys. Res. Lett. 38 (5). https://agupubs.onlinelibrary.wiley.com/doi/abs/10.1029/2010GL046427.

Guan, K., Thompson, S.E., Harman, C.J., Basu, N.B., Rao, P.S.C., Sivapalan, M., et al., 2011. Spatiotemporal scaling of hydrological and agrochemical export dynamics in a tile-drained Midwestern watershed. Water Resour. Res. 47 (10). https://agupubs.onlinelibrary.wiley.com/doi/abs/10.1029/2010WR009997.

Haitjema, H.M., Mitchell-Bruker, S., 2005. Are Water Tables a Subdued Replica of the Topography? Groundwater 43 (6), 781–786. https://ngwa.onlinelibrary.wiley.com/doi/abs/10.1111/j.1745-6584.2005.00090.x.

Jones, J., Woodward, C., 2001. Newton-Krylov-Multigrid solvers for large-scale, highly heterogeneous, variably saturated flow problems. Adv. Water Res. 24, 763–774.

Katul, G.G., Porporato, A., Daly, E., Oishi, A.C., Kim, H.-S., Stoy, P.C., et al., 2007. On the spectrum of soil moisture from hourly to interannual scales. Water Resour. Res. 43 (5). https://agupubs.onlinelibrary.wiley.com/doi/abs/10.1029/2006WR005356.

Kirchner, J.W., Feng, X., Neal, C., 2000. Fractal stream chemistry and its implications for contaminant transport in catchments. Nature 403 (6769), 524–527. https://doi.org/10.1038/35000537.

Kollet, S., Sulis, M., Maxwell, R.M., Paniconi, C., Putti, M., Bertoldi, G., et al., 2017. The integrated hydrologic model intercomparison project, IH-MIP2: A second set of benchmark results to diagnose integrated hydrology and feedbacks. Water Resour. Res. 53 (1), 867–890. https://agupubs.onlinelibrary.wiley.com/doi/abs/10.1002/2016WR019191.

Kollet, S.J., Maxwell, R.M., 2006. Integrated surface–groundwater flow modeling: A free-surface overland flow boundary condition in a parallel groundwater flow model. Adv. Water Res. 29 (7), 945–958. https://www.sciencedirect.com/science/article/pii/S0309170805002101.

Li, Z., Zhang, Y.-K., 2007. Quantifying fractal dynamics of groundwater systems with detrended fluctuation analysis. J. Hydrol. 336 (1), 139–146. http://www.sciencedirect.com/science/article/pii/S0022169407000030.

Liang, X., Zhang, Y.-K., 2013. Temporal and spatial variation and scaling of groundwater levels in a bounded unconfined aquifer. J. Hydrol. 479, 139–145. https://www.sciencedirect.com/science/article/pii/S0022169412010232.

Liang, X., Zhang, Y.-K., 2015. Analyses of uncertainties and scaling of groundwater level fluctuations. Hydrol. Earth Syst. Sci. 12, 1–23.

Liang, X., Zhang, Y.-K., Schilling, K., 2016. Effect of heterogeneity on spatiotemporal variations of groundwater level in a bounded unconfined aquifer. Stochastic Environmental Research and Risk Assessment 30 (1), 1–8. https://doi.org/10.1007/s00477-014-0990-4.

Little, M., Bloomfield, J., 2010. Robust evidence for random fractal scaling of groundwater levels in unconfined aquifers. J. Hydrol. 393, 362–369.

Manfreda, S., 2007. Scaling characteristics of spatial patterns of soil moisture from distributed modelling. Adv. Water Res. 30. vno. 102145-2150-2007 v.2130 no.2110.

Matsoukas, C., Islam, S., Rodriguez-Iturbe, I., 2000. Detrended fluctuation analysis of rainfall and streamflow time series. Journal of Geophysical Research: Atmospheres 105 (D23), 29165–29172. https://agupubs.onlinelibrary.wiley.com/doi/abs/10.1029/2000JD900419.

Maxwell, R.M., 2010. Infiltration in Arid Environments: Spatial Patterns between Subsurface Heterogeneity and Water-Energy Balances. Vadose Zone J. 9 (4), 970–983. https://acsess.onlinelibrary.wiley.com/doi/abs/10.2136/vzj2010.0014.

Maxwell, R.M., 2013. A terrain-following grid transform and preconditioner for parallel, large-scale, integrated hydrologic modeling. Adv. Water Res. 53, 109–117. https://www.sciencedirect.com/science/article/pii/S0309170812002564.

Maxwell, R.M., Condon, L.E., Kollet, S.J., Maher, K., Haggerty, R., Forrester, M.M., 2016. The imprint of climate and geology on the residence times of groundwater. Geophys. Res. Lett. 43 (2), 701–708. https://agupubs.onlinelibrary.wiley.com/doi/abs/10.1002/2015GL066916.

Maxwell, R.M., Putti, M., Meyerhoff, S., Delfs, J.-O., Ferguson, I.M., Ivanov, V., et al., 2014. Surface-subsurface model intercomparison: A first set of benchmark results to diagnose integrated hydrology and feedbacks. Water Resour. Res. 50 (2), 1531–1549. https://agupubs.onlinelibrary.wiley.com/doi/abs/10.1002/2013WR013725.

McColl, K., Alemohammad, H., Akbar, R., Konings, A., Yueh, S., Entekhabi, D., 2017. The global distribution and dynamics of surface soil moisture. Nat. Geosci. 10, 100–104.

Mikkelson, K.M., Maxwell, R.M., Ferguson, I., Stednick, J.D., McCray, J.E., Sharp, J.O., 2013. Mountain pine beetle infestation impacts: modeling water and energy budgets at the hill-slope scale. Ecohydrology 6 (1), 64–72. https://onlinelibrary.wiley.com/doi/abs/10.1002/eco.278.

Özger, M., Mishra, A.K., Singh, V.P., 2013. Seasonal and spatial variations in the scaling and correlation structure of streamflow data. Hydrol. Processes 27 (12), 1681–1690. https://onlinelibrary.wiley.com/doi/abs/10.1002/hyp.9314.

Pandey, G., Lovejoy, S., Schertzer, D., 1998. Multifractal analysis of daily river flows including extremes for basins of five to two million square kilometres, one day to 75 years. J. Hydrol. 208 (1), 62–81. https://www.sciencedirect.com/science/article/pii/S0022169498001486.

Pedretti, D., Russian, A., Sanchez-Vila, X., Dentz, M., 2016. Scale dependence of the hydraulic properties of a fractured aquifer estimated using transfer functions. Water Resour. Res. 52 (7), 5008–5024. https://agupubs.onlinelibrary.wiley.com/doi/abs/10.1002/2016WR018660.

Rahman, M., Rosolem, R., Kollet, S.J., Wagener, T., 2019. Towards a computationally efficient free-surface groundwater flow boundary condition for large-scale hydrological modelling. Adv. Water Res. 123, 225–233. https://www.sciencedirect.com/science/article/pii/S0309170818303701.

Russian, A., Dentz, M., Le Borgne, T., Carrera, J., Jimenez-Martinez, J., 2013. Temporal scaling of groundwater discharge in dual and multicontinuum catchment models.

Water Resour. Res. 49 (12), 8552–8564. https://agupubs.onlinelibrary.wiley.com/doi/abs/10.1002/2013WR014255.

Sauquet, E., Ramos, M.-H., Chapel, L., Bernardara, P., 2008. Streamflow scaling properties: investigating characteristic scales from different statistical approaches. Hydrol. Processes 22 (17), 3462–3475. https://onlinelibrary.wiley.com/doi/abs/10.1002/hyp.6952.

Schilling, K.E., Zhang, Y.-K., 2012. Temporal Scaling of Groundwater Level Fluctuations Near a Stream. Groundwater 50 (1), 59–67. https://ngwa.onlinelibrary.wiley.com/doi/abs/10.1111/j.1745-6584.2011.00804.x.

Schuite, J., Flipo, N., Massei, N., Rivière, A., Baratelli, F., 2019. Improving the Spectral Analysis of Hydrological Signals to Efficiently Constrain Watershed Properties. Water Resour. Res. 55 (5), 4043–4065. https://agupubs.onlinelibrary.wiley.com/doi/abs/10.1029/2018WR024579.

Tessier, Y., Lovejoy, S., Hubert, P., Schertzer, D., Pecknold, S., 1996. Multifractal analysis and modeling of rainfall and river flows and scaling, causal transfer functions. Journal of Geophysical Research: Atmospheres 101 (D21), 26427–26440. https://agupubs.onlinelibrary.wiley.com/doi/abs/10.1029/96JD01799.

Tóth, J., 1963. A theoretical analysis of groundwater flow in small drainage basins. Journal of Geophysical Research (1896-1977) 68 (16), 4795–4812. https://agupubs.onlinelibrary.wiley.com/doi/abs/10.1029/JZ068i016p04795.

Vinnikov, K.Y., Robock, A., Speranskaya, N.A., Schlosser, C.A., 1996. Scales of temporal and spatial variability of midlatitude soil moisture. Journal of Geophysical Research: Atmospheres 101 (D3), 7163–7174. https://agupubs.onlinelibrary.wiley.com/doi/abs/10.1029/95JD02753.

Wu, W., Dickinson, R.E., 2004. Time Scales of Layered Soil Moisture Memory in the Context ofLand–Atmosphere Interaction. Journal of Climate 17 (14), 2752–2764. https://journals.ametsoc.org/doi/abs/10.1175/1520-0442%282004%29017%3C2752%3ATSOLSM%3E2.0.CO%3B2.

Wu, W., Geller, M.A., Dickinson, R.E., 2002. The Response of Soil Moisture to Long-Term Variability of Precipitation. Journal of Hydrometeorology 3 (5), 604–613. https://doi.org/10.1175/1525-7541(2002)003<0604:TROSMT>2.0.CO;2.

Yang, C., Zhang, Y.-K., Liang, X., 2018. Analysis of temporal variation and scaling of hydrological variables based on a numerical model of the Sagehen Creek watershed. Stochastic Environmental Research and Risk Assessment 32 (2), 357–368. https://doi.org/10.1007/s00477-017-1421-0.

Zhang, Y.-K., Li, Z., 2005. Temporal scaling of hydraulic head fluctuations: Nonstationary spectral analyses and numerical simulations. Water Resour. Res. 41 (7). https://agupubs.onlinelibrary.wiley.com/doi/abs/10.1029/2004WR003797.

Zhang, Y.-K., Schilling, K., 2004. Temporal scaling of hydraulic head and river base flow and its implication for groundwater recharge. Water Resour. Res. 40 (3). https://agupubs.onlinelibrary.wiley.com/doi/abs/10.1029/2003WR002094.

Zhang, Y.-K., Schilling, K., 2005. Temporal variations and scaling of streamflow and baseflow and their nitrate-nitrogen concentrations and loads. Adv. Water Res. 28 (7), 701–710. http://www.sciencedirect.com/science/article/pii/S0309170805000266.

Zhang, Y.-K., Yang, X., 2010. Effects of variations of river stage and hydraulic conductivity on temporal scaling of groundwater levels: numerical simulations. Stochastic Environmental Research and Risk Assessment 24 (7), 1043–1052. https://doi.org/10.1007/s00477-010-0437-5.